

# **Metal Oxide-based Gas Sensor Array for the VOCs Analysis in Complex Mixtures using Machine Learning**

**Shivam Singh<sup>1</sup>, Sajana S<sup>1</sup>, Poornima<sup>2</sup>, Gajje Sreelekha<sup>3</sup> Chandranath Adak<sup>3,\*</sup>, Rajendra P. Shukla<sup>4,\*</sup>, Vinayak Kamble<sup>1,\*</sup>**

<sup>1</sup>School of Physics, Indian Institute of Science Education and Research Thiruvananthapuram, 695551 India.

<sup>2</sup>Dept. of CSE, Indian Institute of Information Technology Lucknow, Uttar Pradesh 226002, India.

<sup>3</sup>Dept. of CSE, Indian Institute of Technology Patna, Bihar 801106, India.

<sup>4</sup>BIOS Lab-on-a-Chip Group, MESA+ Institute for Nanotechnology, Max Planck Center for Complex Fluid Dynamics, University of Twente, P.O. Box 217, 7500 AE Enschede, The Netherlands.

## **Abstract**

Detection of Volatile Organic Compounds (VOCs) from the breath is becoming a viable route for the early detection of diseases non-invasively. This paper presents a sensor array with three metal oxide electrodes that can use machine learning methods to identify four distinct VOCs in a mixture. The metal oxide sensor array was subjected to various VOC concentrations, including ethanol, acetone, toluene and chloroform. The dataset obtained from individual gases and their mixtures were analyzed using multiple machine learning algorithms, such as Random Forest (RF), K-Nearest Neighbor (KNN), Decision Tree, Linear Regression, Logistic Regression, Naive Bayes, Linear Discriminant Analysis, Artificial Neural Network, and Support Vector Machine. KNN and RF have shown more than 99% accuracy in classifying different varying chemicals in the gas mixtures. In regression analysis, KNN has delivered the best results with  $R^2$  value of more than 0.99 and LOD of 0.012, 0.015, 0.014 and 0.025 PPM

\*email: [chandranath@iitp.ac.in](mailto:chandranath@iitp.ac.in) ; [r.p.shukla@utwente.nl](mailto:r.p.shukla@utwente.nl) ; [kbyvinayak@iisertvm.ac.in](mailto:kbyvinayak@iisertvm.ac.in)

for predicting the concentrations of varying chemicals Acetone, Toluene, Ethanol, and Chloroform, respectively in complex mixtures. Therefore, it is demonstrated that the array utilizing the provided algorithms can classify and predict the concentrations of the four gases simultaneously for disease diagnosis and treatment monitoring.

**Key words:** Gas sensor array, Metal oxide, Volatile Organic Compound, Complex mixture, Machine learning.

## 1. Introduction

Modern technology is becoming even more essential for applications relating to healthcare. Consequently, there is much interest in reducing surgical involvement and enhancing illness early identification. Since it is quicker, less intrusive, and more accessible than a traditional clinical assessment, identifying certain illnesses employing human exhaled air has garnered great interest[1-3]. In this context, exhaled breath is the ideal non-invasive approach since it accurately captures the metabolic processes occurring within the human body[4, 5]. Compared to standard urine or serum tests, disease identification utilizing expiratory VOCs has emerged as the preferable approach for early screening. Besides, it has another excellent relevance for continuous breath monitoring for knowing health anomalies that appear transient or periodic[6]. Breath monitoring has several benefits, the most significant among them being a simple, quick, and straightforward sampling collection method provided by its non-invasive approach[7]. Many (about hundreds) of volatile chemical molecules are found in an individual's breath[4]. Some Volatile Organic Compounds (VOC) chemicals, notably isoprene (heart disease), acetone (diabetes), toluene (lung cancer), nitrogen monoxide (asthma), pentane (heart disease) and ammonia (kidney dysfunction) are established indicators that anticipate underlying disorders[8-10]. However, as shown in Fig. 1(a), several variables affect the constitution of exhaled breath and can be broadly classified as lifestyle-based, health-based and environment based.

The usual range for toxicants in a person's exhaled breath is between parts per billion (PPB) to parts per trillion (PPT)[11]. The number of VOCs and their relative proportions are specific to the health of individuals, or unexpected VOCs may be released by irregular metabolic reactions[5]. Therefore, breath evaluation is often used to identify various diseases, including renal dysfunction, prostate cancer, and other types of cancers[1, 5, 12]. Identifying various indicators for each ailment makes it possible to distinguish between healthy people and those

with illnesses using a sensor array. It is also possible to continually monitor those using wearable technology[6, 7, 13].

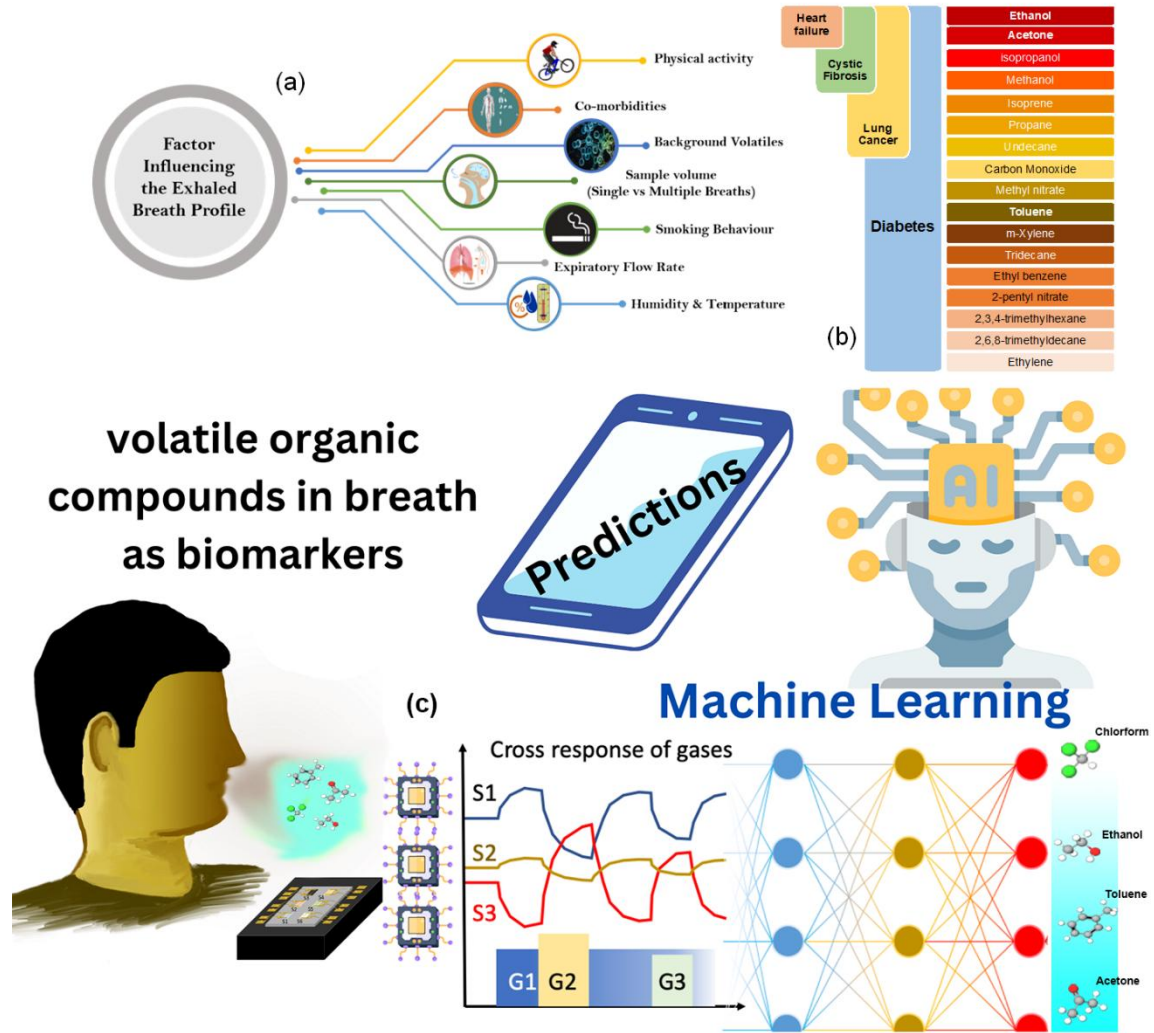


Fig. 1: (a) Variables affecting the exhaled breath composition. (b) Cumulative breath biomarkers linked to cystic fibrosis, lung cancer, heart failure and diabetes (adapted from [14]). (c) The schematic of breath sampling having possible VOCs and sensor array response to a mixture of gases. The AI route to deconvolution complexity of the data and make composition predictions.

The brief involvement of these VOCs in various diseases through exhalation and their severe effect on the human body are expressed in Fig. 1(b). We have identified common VOCs

like ethanol, toluene, acetone, and chloroform, among the biomarkers routinely used to analyze the response. Numerous potential uses, including exhaled condition monitoring for the detection of smaller doses of ethanol, have lately gained considerable attention. Breath ethanol levels in a healthy individual are typically below 380 parts per billion. Nevertheless, this might increase to 2300 ppb in cases of alcoholism and a history of fatty liver[15, 16]. Exhaled Breath includes several volatile chemicals, most present in minimal ppb concentrations. In such circumstances, it is thought that a person who has elevated breath acetone ( $T2DM > 1.71$  ppm,  $T1DM > 2.19$  ppm (Type 1 diabetes mellitus (T1DM), an asymptomatic disease, is caused by the body's antibodies attacking and killing the beta cells that produce insulin in the pancreas. As a result, little or no insulin is created, which causes blood sugar levels to increase. It often affects children and young people, and insulin therapy is always required. However, in type 2 diabetes mellitus (T2DM), the body generates inadequate quantities of insulin or becomes resistant, making it difficult to maintain normal blood sugar levels. Acetone often develops in adults and correlates with lifestyle factors, including obesity and inactivity and it may well go approximately 21 ppm[17, 18], which would ring alarming bells of diabetes. A biochemical disorder like diabetes mellitus affects over 400 million people worldwide[19] linked to such occurrences. Diabetes and disorders with overlapping biomarkers are shown graphically in Fig. 1(b). In humans, breathing indoor air or consuming substantial quantities of chloroform-containing liquids such as chlorinated water may result in the presence of chloroform in breath[20]. Besides, chloroform has been reported to affect the liver, kidneys, and the neurological network in general (brain)[21].

Current-state-of-the-art technologies use gas chromatography followed by mass spectroscopy to analyze breath samples to investigate specific VOCs in patient samples. Although those are precise, these techniques require a sophisticated setup and trained individuals to handle those, increasing the analysis cost. Moreover, it is also a time taking process to get the analysis

report from centralized laboratories. These techniques also use labeling or pretreatment of the samples, which may affect the exact levels of the VOCs in complex media.

Recently, gas sensors have been explored to analyze VOCs in breath samples due to their simple design, high sensitivity, fast response time and cost-effectiveness[22-25]. These sensors can be employed at the point-of-care for VOCs analysis. Metal-oxide-based gas sensors have gained significant interest in these sensors due to their small size, ease of operation, inexpensiveness, excellent sensing performance and low maintenance. However, despite the high sensitivity and fast response time, these sensors have yet to reach clinical studies due to the presence of interfering species generating overlapping and masking gas-sensing signals[26]. The electrical signals generated from the gas sensor in a multi-component mixture solution are difficult to differentiate between signals of the target analyte and interfering species. In the recent past, another approach called "electronic nose" where a gas sensor array has been utilized in place of a single sensor to record the response in a multi-component mixture solution, and the data was analyzed using Machine Learning (ML) algorithms[27, 28]. The gas sensor array consists of non-specific sensors in the array and records the fingerprints of the multi-component mixture solution. This approach reduced the effect of interfering species and required no pretreatment of the breath samples, thereby shifting the challenges of gas sensing from the physical to the digital domain.

In this study, we employed a gas sensor array based on targets that were sputtered with a Direct Current (DC) source to deposit the metal oxides CuO, NiO and ZnO. The responses of various analytes passing over it were recorded using four volatile compounds: ethanol, toluene, acetone, and chloroform. The initial phase was mixing a single analyte with synthetic air and recording the response (resistance vs. time) for each electrode at 200 °C. One electrode was utilized at a time. After that, an experiment was conducted using two gases simultaneously, with one analyte being kept constant at a specific concentration while the other was changed. There were twelve different potential combinations for the 200 °C parallel readings. Similarly,

the reaction was measured while carefully purging three gases, with two maintaining constant and the third changing. The gas sensor array's electrical response was examined using ML techniques. We have used different ML algorithms to analyze the data from the Metal Oxide Semiconductor (MOS) sensor array and compared their performances for the simultaneous detection of four VOCs. The ML algorithm was used to perform two types of analysis: (i) *classification* to categorize the varying gas/ chemical and (ii) *regression* analysis to predict the concentration of the gas. Therefore, not only qualitative but quantitative detection of four VOCs simultaneously allows the detection of multiple diseases and monitoring of the health of individuals. The proof-of-concept demonstration using a sensor array combined with ML algorithms can potentially analyze individual VOCs in breath samples to provide diagnostic and therapeutic information in diseases outlined such as lung cancer, heart diseases, diabetes and fibrosis, etc. Further miniaturization and its application to point-of-care testing devices can improve diagnostics and treatment monitoring of diseases (e.g., cancer).

## 2. Experimental Details

In this section, we discuss the fabrication of MOS gas sensor array followed by experiment setups for ML-based gaseous chemical classification and regression analysis.

### 2.1. Fabricating metal oxide (MOS) gas sensor array

#### 2.1.1. Thin film deposition using DC-RF magnetron sputtering

DC reactive magnetron sputtering was used to create thin films of CuO, NiO and ZnO onto both glass and alumina substrates. During DC magnetron sputtering, the metal (Copper, Nickel, and Zinc) targets (99.99%) of 1 inch in diameter and a few millimeters thick were employed. The sputter gas was pure argon (99.9997%), while the reactive gas was pure oxygen (99.9997%). Mass flow regulators controlled both gas-flows independently. The sputtering chamber was vacuumed to a base pressure of about  $10^{-6}$  mbar with the help of a turbo molecular

vacuum pump and a rotary mechanical backing pump before the thin oxide films were deposited. The input parameters of different voltages and currents were used. The constant Argon flow rate was 30 SCCM. Pre-sputtering was kept going for 10 minutes to ensure the target surface was thoroughly scrubbed. Following the pre-sputtering step, 10 SCCM of oxygen was added into the reaction chamber while the deposition pressure was maintained at a constant  $\sim 10^{-2}$  mbar. Thin film deposition on substrates may begin once the shutter is opened. The optimum deposition time ( $t_d$ ) was different for three oxides, while the optimum substrate temperature ( $T_s$ ) was 300 K. After rotating the substrates while maintaining a distance of 6-8 cm from the target, we found the best results. Table S1 shows the variation of deposition parameters for all three oxide films. The sputtered samples are shown digitally in Fig. S1(insert).

### **2.1.2. Material characterization of MOS gas sensor array**

Powder X-ray diffraction (XRD) was used to examine the microstructure and crystallinity of materials using a Bruker Powder XRD device utilizing Cu  $\text{k}\alpha$  radiation ( $\lambda = 1.5418 \text{ \AA}$ ) and a nickel filter. Data were gathered at a scan rate of 2 data points per minute, with steps of 2 thetas ranging from 10 to 80 degrees. The films' surface morphology was captured using a Nova NANOSEM 450 equipped with WDS and EDS. We used a secondary emission mode with an operating voltage of 10 kV for this particular picture capture. EDS was used to verify the composition of the elements. Raman spectroscopy was performed with a Horiba scientific Xplora plus spectrometer using a 514-nanometer-wavelength argon laser. The samples' thickness was determined using a KLA Tencor D600 stylus surface profiler equipped with a step height measuring system.

### **2.1.3. Gas sensing studies using MOS sensor array: Experimental setup**

Gas sensing experiments were carried out by observing how the thin films' electrical resistance changed in response to various VOCs at fixed operating temperatures. The sample

gases were infused under dynamic flow conditions fixed by mass flow controllers (Maker Alicat, United States) with varying capacities. In order to create the test gas vapors, synthetic air was bubbled over volatile organic compounds that were maintained at a constant heating of zero degrees Celsius by an MFC-controlled carrier gas flow. The vapor concentrations were calculated using the Antoine equation. It could adjust the dilution factors by combining the test gas-saturated transport fumes with a synthetic flow of air that the MFC sustains.

Fig. S2 depicts the gas detection apparatus used in this investigation. The films were mounted on a brass sample holder and put in a detecting chamber that could reach 400 °C using a calibrated smart thermostat (Excel Instruments) to evaluate the gas sensing characteristic. A thermocouple of class K was subsequently inserted into the film frame and connected to the thermometer to measure the sensor's temperature. An Alumina substrate with interdigitated Gold electrodes is utilized for measuring sensor resistance. A Keithley 6517B electrometer linked to a workstation was used to measure the sensor resistance by applying a consistent bias voltage of 10 V to two probes. With a tolerance of 1 fA, it's a high-resistance analyzer that could contribute meaningfully to  $10^{15}$  ohms. Exposing the deposited films to the appropriate vapours diluted in air was necessary to test the sensor response for ethanol and other volatile organic chemicals. The % response (S) was calculated using eq (1) as below.

$$\% \text{ Response}, S = \frac{Ra - Rg}{Ra} \quad (1)$$

Where Ra is the sensor resistance within airflow and Rg is the sensor resistance when the test gas is present. It should be noted that the response sign for n-type and p-type devices is opposite to the stated gas. The sensor resistance decreases when n-type material is exposed to a reducing gas because the gas injects excess carriers into the material. However, as the resistance decreases, the resistance changes the most, increasing 100% monotonically. However, suppose the resistance increases due to gas exposure, as in the case of p-type material subjected to

reducing gas. In that situation, the standard deviation of the resistance change is more significant than 100% or greater than double the original value.

The chemiresistive array sensing tests were done by passing a set amount of target gas mixed with a predefined proportion of air, determined by the equalization method at fixed intervals. Both with and without the analyte, the total flow was maintained at 500 SCCM, and the two-probe mode was used to collect the sensor's resistance data. The sensors were tested by being exposed to ethanol concentrations of 100–2400 ppm at 200 °C. Individual response research utilizing toluene, chloroform, and acetone was also carried out under identical conditions. By cooling the liquids in the tube to the same temperature and using the same MFC dispersion ratios, similar studies were conducted at 200 °C to examine ethanol's cross-sensitivity to other gases such as toluene, chloroform, and acetone.

## **2.2. Gaseous chemical classification and regression analysis using machine learning models**

The dataset used in this study consists of gas sensor data comprising three different mixtures. Each mixture represents a distinct scenario based on the number of gases present, namely

- i. *1-gas*: a single gaseous chemical,
- ii. *2-gases*: mixture with one constant chemical and one varying chemical,
- iii. *3-gases*: mixture with two constant chemicals and one varying chemical.

The chemicals involved in these mixtures are Acetone, Toluene, Chloroform, and Ethanol. On these 1-gas, 2-gases and 3-gases datasets, we performed the analysis. All possible combinations of four biomarkers were employed to record the readings for the mixtures with two and three gases, mentioned in Table S2. A gaseous chemical that needs to be classified or whose

concentration needs to be anticipated is kept variable for datasets with mixtures of gases. Three sensing components (CuO, NiO, and ZnO) are used in the dataset to record measurements. The objective is to predict or classify the concentration of the varying gas, whether it is Acetone, Toluene, Chloroform, or Ethanol.

Each dataset has the following sample rows: 2241436 sample rows for 1-gas, 227617 rows for the mixture of 2-gases and 131120 rows for the mixture of 3-gases. There are 6, 8, and 10 columns in the abovementioned datasets. The correlation matrices for the three datasets are shown in Fig. S3 in supplementary information. We performed two types of analysis: (i) *classification* to categorize the varying gas/ chemical and (ii) *regression* analysis to predict the concentration of the gas.

For the classification task with 1-gas dataset, we used five features, i.e., resistance, time, concentration in terms of parts per million (PPM), temperature and electrode, to categorise the varying chemicals. For the classification task with 2-gases dataset, we used seven features, i.e., time, ZnO\_resistance, NiO\_resistance, CuO resistance, constant\_chemical (CC), CC\_PPM and varying\_chemical\_PPM (VC\_PPM) to classify varying\_chemical (VC). For 3-gases dataset, we used nine features, i.e., time, ZnO\_resistance, NiO\_resistance, CuO resistance, constant\_chemical\_1 (CC\_1), CC\_1\_PPM, CC\_2, CC\_2\_PPM, and varying\_chemical\_PPM to classify varying\_chemical (VC). For regression tasks with 1-gas, we predicted the gas concentration in PPM; for both of the 2 and 3 gases datasets, we predicted VC\_PPM. The rest of the column values were used as features. For the experimental analysis, the dataset was divided into training, validation and testing sets with a ratio of 56:14:30. To assess the performance of the classification analysis, the accuracy metric was used; and for the regression analysis, the mean absolute error (MAE), mean squared error (MSE), root mean square error (RMSE), normalized RMSE (NRMSE), coefficient of determination ( $R^2$ ), Limits of Detection

(LoD), and Limit of Quantification (LoQ) were employed[29-31]. Here, we present the results of the test dataset.

We observed significant outliers in the dataset. Outliers in the input data may distort and deceive ML models during training, leading to longer training times, less accurate models and ultimately worse outcomes. Therefore, the outliers were eliminated using the data quantile information[31] defining an upper and lower limit. A data value was eliminated from our primary data frame if it exceeded the upper limit or fell below the lower limit. The datasets underwent preprocessing steps to conduct a comprehensive analysis, including outlier detection and removal, min-max scaling to handle variations in feature values and label encoding to address categorical features[32]. Categorical data[33] was encoded using label encoding, as only eight distinct values were in the categorical column. It is crucial to convert categorical data into a numerical format to enable processing by ML models. Other approaches for categorical data include one-hot encoding, vectorization and label encoding. Upon completing the dataset preprocessing, models were built using the selected algorithms. Rigorous hyperparameter tuning was performed for all the algorithms employed in this gas sensor dataset analysis. Grid search cross-validation was utilized for hyper parameter tuning[34].

**Machine configuration:** All the ML based analysis were performed on the TensorFlow-2 framework having Python 3.7.13 over a computer with Intel(R) Xeon(R) CPU @ 2.00GHz having 52 GB RAM and Tesla T4 16 GB GPU.

### 3. Results

This section discusses the fabrication of devices, characterization of gas sensor array, ML-based classification and regression of gaseous chemicals.

### **3.1. Device fabrication, characterization of the gas sensor array and sensing studies**

In order to create our device, we used a DC reactive magnetron sputtering technique to deposit copper, nickel, and zinc oxide on an alumina substrate having interdigitated gold electrodes with the corresponding metal targets. Table S1 represents the sputtering parameter to ensure the deposition process is accurate. Pre-deposition of 10 minutes was done to ensure that the surface was thoroughly scrubbed and no contamination was left. Fig. S1 (inset) represents the schematic diagram of our fabricated device. The gold electrodes were vital because they helped the device detect resistance changes when exposed to different gases.

#### **3.1.1. Material characterization of MOS gas sensor array**

Although the samples used in gas sensing are deposited on Alumina substrates, the XRD of those films was primarily dominated by highly crystalline Alumina substrate peaks. Therefore, to confirm the crystallinity of each synthesized sensor film, the same were also deposited on glass and investigated using XRD. The corresponding XRD patterns of CuO, NiO, and ZnO are displayed in Fig. 2(a). The bottommost XRD data in Fig. 2(a) illustrates the characteristic patterns for the (002), (-111) and (111) reflections of a monoclinic CuO layer with lattice constants of 5.13, 3.42, and 4.68 Å (JCPDS: 01-073-6023). Similarly, the (111) and (200) considered as the top of NiO (JCPDS: 00-047-1049) were matched by the middle XRD pattern, which corresponds to a cubic arrangement with lattice constants of  $a = b = c = 4.17$  Å. The top-most XRD pattern in Fig. 2(a) shows a single peak that matches the ZnO wurtzite structure containing positions (100), (002) and (101) (JCPDS: 00-036-1451), and it possesses a hexagonal structure with cell parameters ( $a = b = 3.25$  and  $c = 5.21$  Å). No extra peaks corresponding to any impurity are seen to the best of the resolution in any of the XRD patterns. From all these XRD data, it may be inferred that each of the oxide layers is formed albeit with a minimal thickness which results in the poor intensity of peaks and primarily ZnO and NiO show a very strong texture in crystallinity marked by a single diffraction peak. This implies

that the films are preferentially oriented (except CuO) along a certain direction<sup>22</sup>. This happens due to homogeneous nucleation of the oxide crystals, which grow along the crystal's energetically most favorable (lowest formation energy) planes. Moreover, the broadening of the peaks reflects a smaller crystallite size, possibly due to a lack of energy for long-range growth as the deposition is carried out at room temperature. Nevertheless, such small crystallite size and low thickness are favorable for gas sensing as the sensing response is dramatically improved if the dimensions are of the order of space charge region[35].

Because of the low thickness of the films, the XRD pattern is not significant in analyzing the crystallinity of the films. Therefore, Raman spectra have been investigated for all three samples at room temperature. Here the signal is collected from the tiny focus of the laser beam on the film surface and is collected in back reflection geometry. Therefore, it has much better sensitivity to the surface than the substrate that lies below. The Raman spectra identify their vibrational properties at ambient temperature and are found to give peaks that are unique to each material. The copper oxide Raman spectrum on an alumina substrate is shown in Fig. 2(b), depicting Raman modes at 294.38, 343.3, and 628.8  $\text{cm}^{-1}$ . The positions of the peaks in the spectra with this specimen are in close vicinity of those corresponding reported CuO values[36, 37]. Several factors, such as poor crystallinity, an accumulation of structural faults in the crystalline lattice, and fluorescence of the incident radiation, may be responsible for the broad baseline around 400 and 600  $\text{cm}^{-1}$  seen in this spectral region.

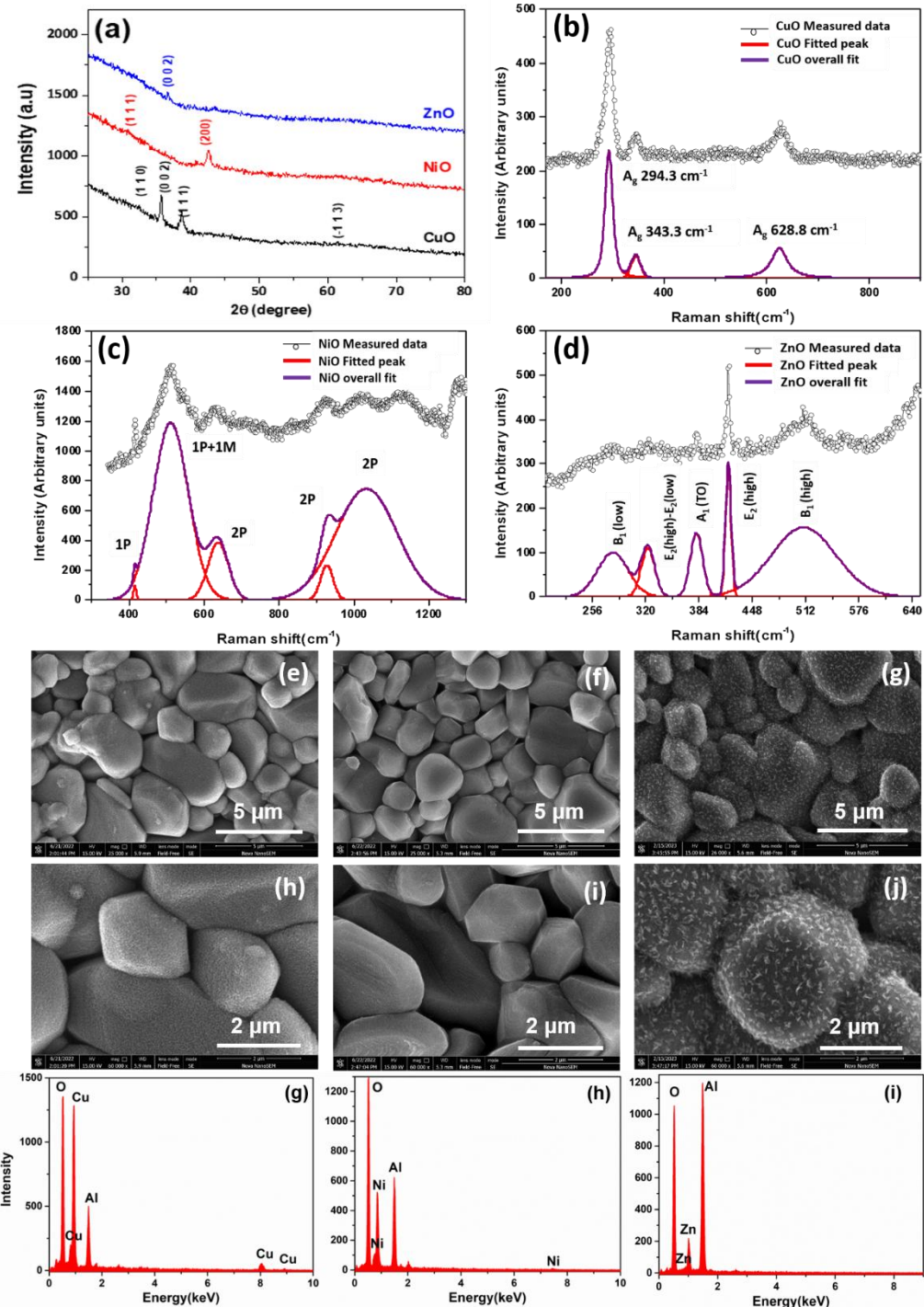


Fig. 2: The (a) XRD patterns and Raman spectra of (b) CuO, (c) NiO and (d) ZnO of the thin films at room temperature (for XRD, the samples were also deposited on glass substrates). The Scanning electron micrographs of CuO, NiO and ZnO at low (e-g) and high (h-j) magnifications, respectively. EDS spectra of (k) CuO, (l) NiO and (m) ZnO.

Fig. 2(c) depicts the Raman spectra recorded for NiO thin films that were deposited on a glass substrate for 18 minutes. As per identification in ref[38], the peaks observed may be ascribed to the one-phonon (1P) (at  $570\text{ cm}^{-1}$ ) constituting TO and LO modes, (2P) 2TO aspects (at  $730\text{ cm}^{-1}$ ), and 2LO modes (at  $1090\text{ cm}^{-1}$ ), respectively, thereby confirming the phase. The moderate fraction of 2TO (at  $730\text{ cm}^{-1}$ ) equates to a two-phonon (2P) transverse sequence. In comparison, the peaks LO at  $570\text{ cm}^{-1}$  and 2LO at  $1090\text{ cm}^{-1}$  relate to longitudinal optical phonon modes (LO) of a primary and secondary order, respectively. The Ni-O bond's stretching mode and flaws are both indicated by the peak LO's considerable breadth ( $570\text{ cm}^{-1}$ )[39].

The Raman modes A1(TO) positioned at  $380\text{ cm}^{-1}$ , E2(H) at  $435\text{ cm}^{-1}$  and ELO at  $583\text{ cm}^{-1}$  constitute the vibrational configurations corresponding to the hexagonal wurtzite geometry of ZnO[35, 40] on an alumina surface, as shown in Fig. 2(d). Although the peak at  $325\text{ cm}^{-1}$  matches up to the second order vibration mode originating from the zone boundary phonons [ $E_{2(\text{high})}-E_{2(\text{low})}$ ] of hexagonal ZnO[35], 2LA pattern ( $536.4\text{ cm}^{-1}$ ) correlates to Longitudinal Acoustic (LA) phonon vibration of the second order. The sharp peak at  $418\text{ cm}^{-1}$  is attributed to ZnO's E1 (TO) state because of the oxygen deficiencies or zinc interstitials. According to Ristic et al.[41], this peak is often found in bulk ZnO grains. The peak at  $510.75\text{ cm}^{-1}$  corresponds to the primary Raman signal of the ZnO A1L weak mode in the wurtzite structure.

Overall, the three samples' Raman spectra show very low intensities and significant peak broadening. Like XRD, this broadening results from the sufficiently small size of the crystallites. Therefore, these results are in good agreement with that of the XRD of the films. However, show better confirmation of single-phase oxide films and their nanocrystalline nature.

Along with the crystalline structure, the morphology (shape, grain size, porosity, etc.) of the sensor films significantly affects the sensing attributes of the chemiresistive sensors. Therefore, the microstructure and morphology of the films are examined using scanning electron microscopy along with microscopic composition analysis using energy dispersive X-ray spectroscopy. The same for all three films is shown in Fig. 2(e)-2(j) at low and high magnifications. It should be noted that the films are deposited on a polycrystalline Alumina substrate that has a distinct grain structure. The same is seen in SEM images of all the films. However, the sensing oxide film deposited on its top takes an almost conformal shape of the alumina substrate grains. It, therefore, is not easily seen at low magnification (Fig. 2(e,f,g)).

Upon close inspection at high magnifications, the smaller crystallites of the sensing oxide are seen in all three films (Fig 2. (h, i, j)). It may be seen that the particles are clustered, making it exceedingly difficult to determine their form. The granules develop in tiers, and the texture appears rough. Nevertheless, such a high surface roughness and thereby, high surface area is beneficial for the gas sensing devices. The ZnO films particularly show a 2D flake-like morphology. Typically ZnO sheets, when formed, have (002) orientation due to the low free energy of formation[42]. The presence of sheets along with (002) a single peak in XRD points to the same.

The local chemical composition of the films is examined through EDS spectroscopy. It may be seen from Fig. 2 (k, l, m) that along with the Al form substrate, only a single metal is seen in the spectra of each film such as Cu, Ni and Zn. While the oxygen peak may arise from sensor film or substrate as both are oxides.

### **3.1.2. Electrical Measurement of the MOS gas sensor array**

The I-V characteristics of the oxide thin films deposited in the alumina substrate with gold IDEs were investigated from room temperature to 300 °C. The bias voltage was swept

between -10 V and +10 V to each sensor at ambient temperatures demonstrating an ohmic contact throughout the entire temperature range. The resistance values at each temperature were calculated from I-V slopes. Fig. S4(a, d), S4(b, e) and S4(c, f) show the IV plots for CuO, NiO and ZnO in linear and logarithmic scales. The resistance values so deduced were plotted as a function of temperature, and all the samples demonstrated typical insulating/semiconducting nature. (See Fig. S5 in the supporting information section). The typical value of resistances was about  $500\text{ k}\Omega$ ,  $20\text{ M}\Omega$  and  $100\text{ M}\Omega$  for CuO, NiO and ZnO, respectively, at room temperature. These dropped to  $423\text{ }\Omega$ ,  $14\text{ k}\Omega$ , and  $684\text{ k}\Omega$  at  $300^\circ\text{C}$  for CuO, NiO, and ZnO, respectively.

Here, CuO and NiO are p-type semiconductors, while ZnO is an n-type semiconductor. The typical carrier type in these binary oxides arises because of particular defect chemistry[43-46]. The p-type oxides have metal vacancies whereas n-type oxides have oxygen vacancies as the dominant type of defect. These give rise to the acceptor and donor levels within the forbidden gap respectively. In this case, the thin film fabrication was done under significant oxygen partial pressures (30:10 SCCM of Ar and  $\text{O}_2$  ratio). It ensures high lattice oxygen content in films, increasing metal vacancies for p-type and reducing oxygen vacancies for n-type. Therefore, the p-type films are more conducting than the n-type oxides under oxygen-rich deposition conditions[46].

### **3.1.3. Gas Sensing Measurements and data curation**

In order to generate the response dataset for the gas sensor array with response to selected gases, a large number of experiments were performed. Here, sensor temperature, gas concentration and gas type have been identified as primary parameters for the sensor output.

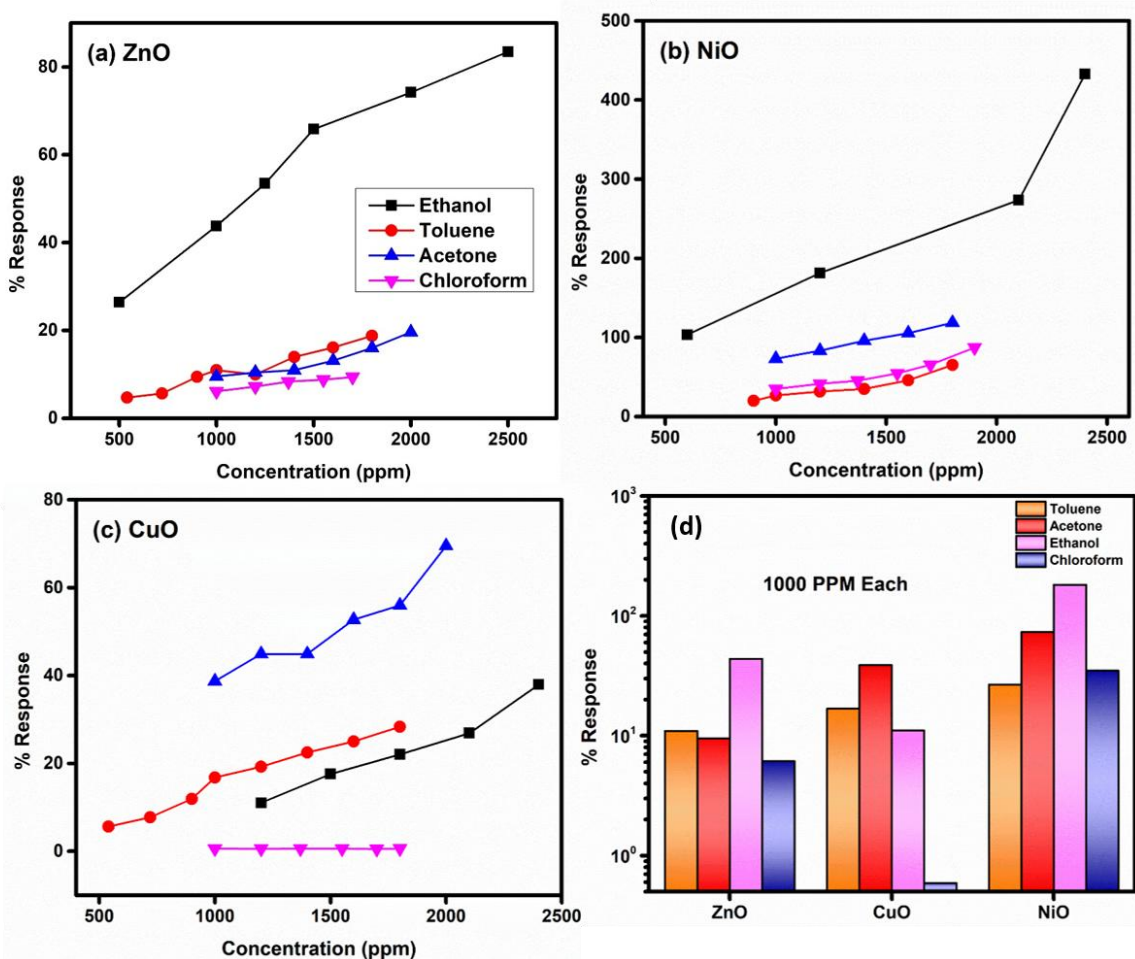


Fig. 3: The individual gas sensing results for four test gases, Toluene, ethanol, acetone and chloroform of the three samples (a) ZnO, (b) NiO and (c) CuO at 200 °C. (d) The comparison of the response for 1000 ppm of each gas for each of the sensing electrodes showing a preferred selectivity for ethanol in NiO and ZnO whereas CuO sensor does not show any preferred selectivity.

As seen in Fig. 3(a-c), the gas sensor's response was calculated and plotted for each gas at different concentrations. Overall, NiO showed a highly selective response to ethanol but a high response to all the gases. At the same time, ZnO had a consistently low response yet was selective to ethanol (See Fig. 3(d)). The actual data sets are shown in the Supporting information section Fig. S6. The consistently high response NiO may be attributed to their

commensurate (low and high) defect concentrations respectively, as defects provide an active site for surface oxygen adsorption[47, 48].

The single gas experiment results shown in Fig. S6 are straightforward and are similar to how traditional gas sensors are reported. However, as mentioned earlier, detecting test gases becomes challenging in the presence of other potentially interfering gases. The experiments were designed such that a predetermined concentration of the interfering species is first supplied as a background flow in the chamber, followed by the introduction of the test gas (2-gases) in order to assess the impact of the interfering species (other gas) on the primary analyte (test gas ethanol). Calculations were made using the response values after varying the test gas concentration. The two interfering gases were maintained constant in the next series of trials (3-gases) while the test gas concentration was altered. The representative data for ethanol response in chloroform (2-gases) and in Toluene + chloroform (3-gases) have been shown in Fig. 4(a and b). The other data sets have been shown in the Supporting information section Fig. S7 & Fig. S8 for 2 gas and 3 gas, respectively. The values of response calculated here for 2-gases and 3-gases depict that the presence of any other VOCs led to a drastic reduction in response. The representative data for NiO response in the absence & presence of a single interfering gas and a double interfering gas is shown in Fig. 4(c and d) respectively. Similar results are obtained when the treatment is done for other sensors and/or permutation – combinations of the gases. The supplementary section Fig. S9 contains the response vs concentration data for CuO and ZnO.

Therefore, analyzing complex mixtures of gases requires non-linear data processing. Hence, we have employed ML algorithms for classification and regression analysis. The results are presented in subsequent sections.

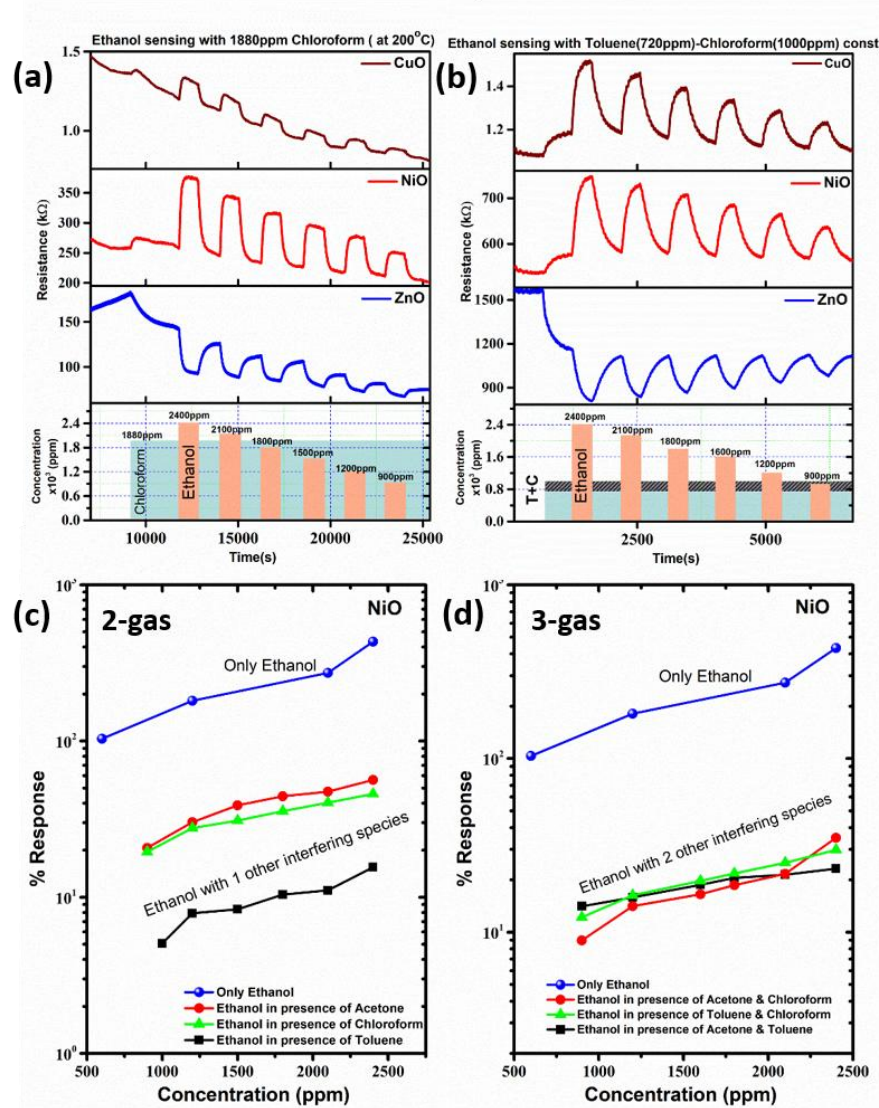


Fig. 4: The response to one gas present alongside another was investigated for all possible combinations. Fig. 4(a) illustrates ethanol sensing in chloroform and 4(b) represents ethanol sensing in chloroform & toluene, at 200 °C. Fig. 4(c) and 4(d) show the computed response values for NiO in the absence & presence of a single interfering gas and a double interfering gas, respectively.

### 3.2. Classification and regression analysis of gases using machine learning

#### 3.2.1. Gas classification

To reduce the complexity of the data while preserving trends and patterns, we used Principal Component Analysis (PCA)[49] on the sensor signal response. The variances of first 5

principal components (PC1, PC2, PC3, PC4, and PC5) are shown in Table S3 for 1-gas, 2-gases and 3-gases datasets. Pictorial representation of variability of first 5 PCs have been shown in Fig. S10.

Here, we formulated the task as a classification problem to classify the gaseous chemicals, i.e., Acetone, Toluene, Chloroform, and Ethanol. The classification models were developed using some supervised learning techniques, e.g., Logistic Regression[47], K-Nearest Neighbor (KNN)[48], Naïve Bayes (NB)[50], Random Forest (RF)[51] and Linear Discriminant Analysis (LDA)[52], based on the PCA results for the gas classification. Different plotted points were dispersed depending on the type of chemicals used as shown in Fig.s S11-S12 and Fig. 5. By taking into account PC1 and PC2, we obtained the 2D plots of Fig.s S11-S12 and Fig. 5 over three datasets. In this instance, PC1, PC2, and PC3 were also employed to produce 3D graphs. In logistic regression[47], the training procedure employed the one-vs-rest scheme since our task involves multiple classes. We used cross-entropy loss and L2 regularization here[53]. In KNN[48], empirically the number of nearest neighbors was set to five, and the distance metric was chosen as Euclidean. In NB[50], every pair of features is conditionally independent given the class variable value, which is a supervised learning technique based on Bayes' theorem. In order to classify our data, we employed the Gaussian Naïve Bayes method. The RF and Extra-Trees methods are two averaging algorithms based on randomized decision trees that we employed[51]. Each algorithm uses a perturb & combine method that is tailored for trees. It means adding randomization to the classifier design results in creating a diverse group of classifiers. The average forecast of the individual classifiers is used to represent the ensemble prediction. Using Bayes' rule and fitting conditional class densities to the data, LDA[52] produces a linear decision boundary for classification. The model assumes that all classes have the same covariance matrix and fit a Gaussian density to

each class. Fig. S11-S12 and Fig. 5 display the 2D and 3D plots of the three datasets obtained after classification using the above-employed methods.

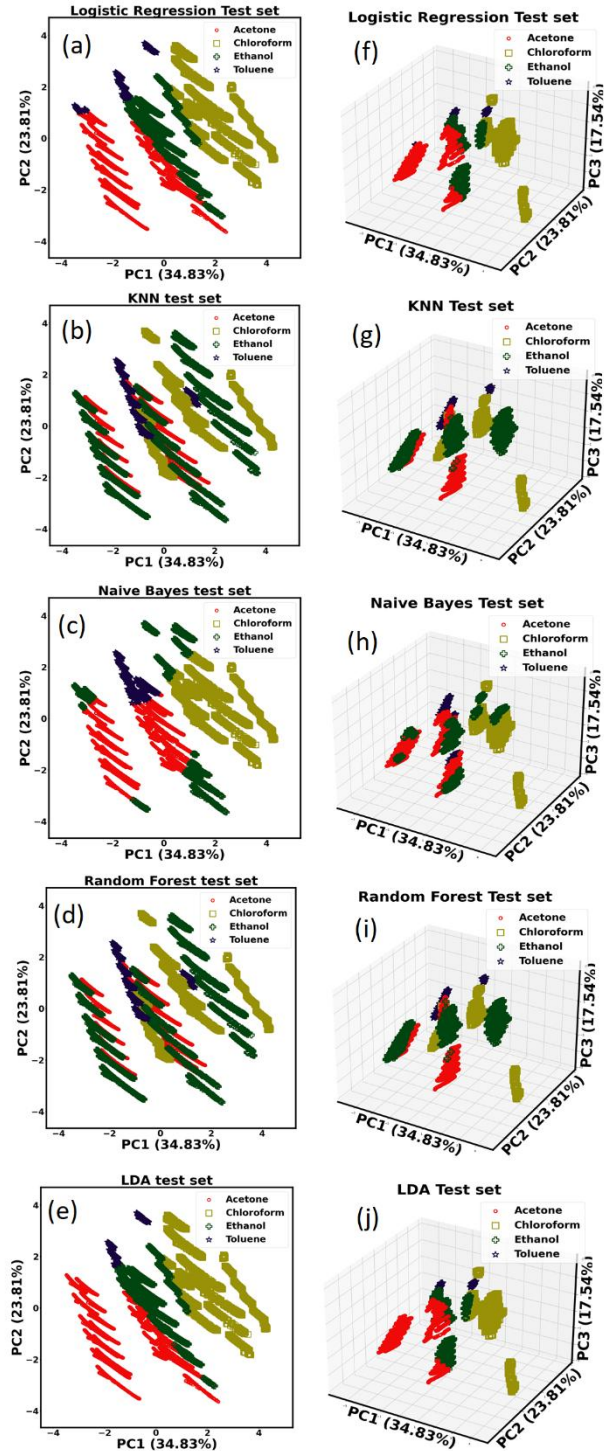


Fig. 5: 3-gases dataset: (a-e)2D and (f-j) 3D classification plots in 1<sup>st</sup> and 2<sup>nd</sup> columns respectively.

In Table 1, we present the accuracies obtained by the employed models. Here, KNN and random forest attained good accuracies for all three datasets, in contrast to the ML models like logistic regression, NB and LDA. For 1-gas and 2-gases datasets KNN performed the best, and random forest attained the best result for the 2-gases dataset instead of their akin performances.

Table 1: Model performances over various gas mixture datasets

A cc	Model Dataset	Logistic Regression	KNN	Naïve Bayes	Random Forest	LDA
ur	<b>1-gas</b>	65.56543	<b>99.99802</b>	71.75669	99.99679	60.06396
ac	<b>2-gases</b>	42.21952	99.81154	60.93418	<b>99.82108</b>	39.78625
y ( % )	<b>3-gases</b>	38.73490	<b>99.03290</b>	51.83471	98.70436	39.76216

In Fig. S11-S12 and Fig. 5, we can also comprehend misclassification results produced by logistic regression, NB, and RF. For example, in Fig. 5 bottom-left, it can be seen that the Ethanol part has been misclassified as Acetone.

### 3.2.2. Regression analysis: quantification of gases in different mixtures

In this analysis, we found that the KNN-based regression[54] significantly exceeded the other algorithms in terms of performance when compared with some other contemporary models, such as Artificial Neural Network (ANN), RF, Decision Tree, and Linear Regression[51, 53-

56]. The performance of the KNN relies on various parameters, such as the distance metric used to evaluate similar data points, the number of neighbors taken into consideration, and the weighting method used to aggregate their values. In this study, we attempted to enhance the effectiveness of the KNN in estimating the gas concentration in mixes. In order to decrease MSE and increase the  $R^2$ , which gauges how much variance can be explained by the model, we set out to identify the optimal set of parameters.

To fine-tune the model, we experimented with various distance metrics, such as Euclidean, Manhattan and Minkowski, with  $p=3$  and  $p=4$ [34]. We used two weighting schemes: distance and uniform, wherein closer neighbors have a higher weight, and we adjusted the number of neighbors taken into consideration, ranging from 1 to 10. The model's performance was checked by applying cross-validation on the training and validation sets, and the optimum set of parameters was decided based on the parameters with the lowest MSE and optimum  $R^2$ . During the hyper parameter tuning procedure for the KNN regression, the best parameter choices for each gas mixture were identified. For all the datasets, i.e., 1-gas, 2-gases, 3-gases, the Euclidean distance metric, the five nearest neighbors, and distance weighting were the most efficient choices. Encouraging results were obtained while analyzing the algorithm's performance with all these ideal parameter configurations.

Table 2: Prediction performance of KNN regression on 1-gas, 2-gases, and 3-gases datasets.

<b>Datas et</b>	<b>Gas Name</b>	<b>RMS E</b>	<b>MSE</b>	<b>MAE</b>	<b>NRMS E</b>	<b><math>R^2</math></b>	<b>LoD</b>	<b>LoQ</b>
1-gas	Acetone	0.0008 6	$7.43 \times 10^{-7}$	0.0000 1	0.0011 4	0.99997	0.0034 4	0.01146

	Toluene	0.0008 2	$6.77 \times 10^{-7}$	0.0000 1	0.0010 9	0.99997	0.0032 8	0.01095
	Ethanol	0.0007 6	$5.82 \times 10^{-7}$	0.0000 1	0.0010 1	0.99997	0.0030 4	0.01015
	Chlorofor m	0.0015 3	$2.35 \times 10^{-6}$	0.0000 4	0.0020 3	0.99990	0.0061 1	0.02039
2- gases	Acetone	0.0013 1	$1.72 \times 10^{-6}$	0.0000 2	0.0031 9	0.99996	0.0095 7	0.03190
	Toluene	0.0009 4	$8.98 \times 10^{-7}$	0.0000 1	0.0022 6	0.99998	0.0067 8	0.02260
	Ethanol	0.0009 5	$9.21 \times 10^{-7}$	0.0000 1	0.0023 0	0.99998	0.0069 2	0.02309
	Chlorofor m	0.0019 4	$3.79 \times 10^{-6}$	0.0000 6	0.0046 6	0.99992	0.0140 0	0.04669
3- gases	Acetone	0.0016 3	$2.67 \times 10^{-6}$	0.0000 5	0.0039 3	0.99994	0.0117 9	0.03932
	Toluene	0.0020 4	$4.19 \times 10^{-6}$	0.0000 6	0.0049 6	0.99991	0.0148 8	0.04961
	Ethanol	0.0019 6	$3.87 \times 10^{-6}$	0.0000 5	0.0047 4	0.99992	0.0142 2	0.04742

	Chlorofor m	0.0034 2	$1.17 \times 10^{-5}$	0.0002 0	0.0082 5	0.99976	0.0247 8	0.08260
--	----------------	-------------	-----------------------	-------------	-------------	---------	-------------	---------

Table 2 presents the prediction performances of KNN regression on 1-gas, 2-gases, and 3-gases datasets, respectively, regarding RMSE, MSE, MAE, NRMSE, R2, LoD, LoQ. The model successfully predicted the target variable for the 1-gas mixture with  $R^2$  of more than 0.99, showing its high prediction performance. Also, it was determined that the corresponding errors (RMSE, MSE, MAE, and NRMSE) were shallow. The model also obtained an outstanding  $R^2$ , i.e., greater than 0.99 for the 2-gases and 3-gases mixtures, implying a solid connection between observed and predicted values. Also, errors were near zeros, implying comparatively smaller magnitudes of the prediction mistakes. The model also excelled in other performance metrics, e.g., LoD and LoQ, when examined on the instances of the 1-gas, 2-gases and 3-gases datasets.

In Fig. 6, we present the regression plots obtained using KNN regression, where the x and y axis denote expected and obtained chemical concentrations separately for Acetone, Toluene, Ethanol and Chloroform over 1-gas, 2-gases, and 3-gases datasets.

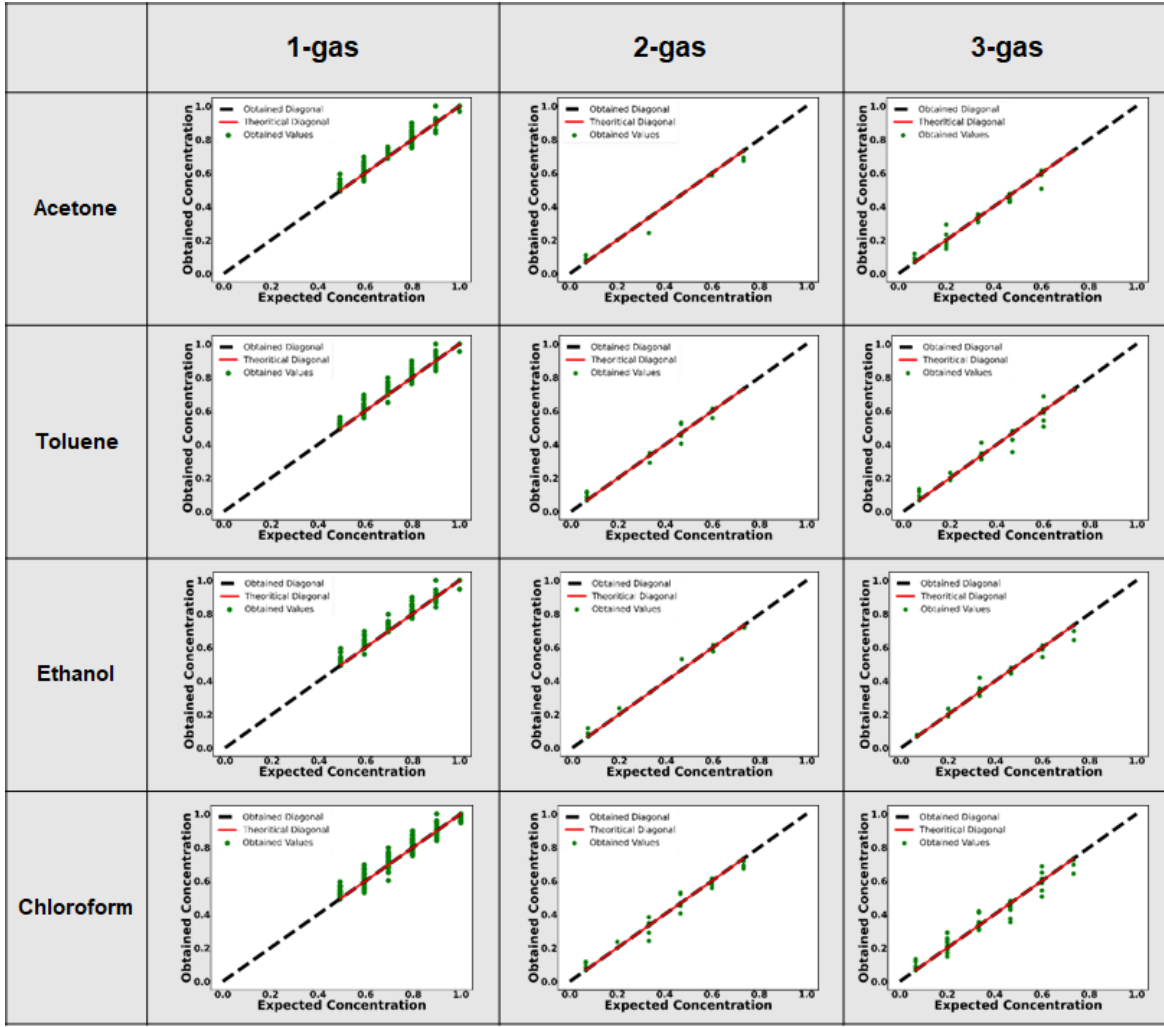


Fig. 6: Prediction plots of KNN regression: 1st Column: 1-gas dataset, 2nd Column: 2-gases dataset and 3rd Column: 3-gases dataset. Row-wise, the prediction of Acetone, Toluene, Ethanol and Chloroform respectively.

As mentioned earlier, we have used ANN, Random Forest, Decision Tree, and Linear Regression for comparative prediction analysis. The ANN can learn and adapt to new data, making it a powerful tool for solving complex problems. However, ANN requires a lot of data and computational power to train and optimize, and its results may only sometimes be interpretable. Here, in the ANN model, we had one neuron on the output layer that matched the concentration of the varying gas. The model comprised six hidden layers containing 128,

256, 512, 64, and 32 neurons. All hidden layers employed the ReLU (Rectified Linear Unit) activation function to capture the non-linearity[57]. We utilized a linear activation function in the output layer. The learning parameters for the ANN model were optimized on the training set using the Adam optimization function. Here, the training effectiveness was assessed using the loss function MSE. The following hyper-parameters were empirically fixed on the validation set: learning rate =  $10^{-3}$ , Adam's first and second moment estimates 0.9 and 0.999, and zero-denominator remover =  $10^{-7}$ .

In linear regression[55], we model the relationship between the dependent and one or more independent variables. Here, we identify the line of best fit that minimizes the sum of squared errors between the predicted and actual values. In decision tree regression[56], we use a tree-like model of decisions and their possible consequences for prediction. However, they can be prone to overfitting and may need to be more accurate in certain situations. Random forest[51] ensembles multiple decision trees to improve performance and reduce overfitting. It randomly selects a subset of features and data samples for each tree to make it robust to noise and outliers. It also offers feature importance ranking and can handle missing data. However, it may perform poorly on imbalanced datasets and can be computationally expensive for large datasets.

In Tables S4, S5 and S6, we compare the experimental results obtained on 1-gas, 2-gases and 3-gases datasets using KNN regression, ANN, random forest, decision tree, and linear regression models. The evaluation results regarding metrics RMSE, MSE, MAE, NRMSE,  $R^2$ , LoD and LoQ are shown here for predicting Acetone, Toluene, Ethanol, and Chloroform gases. Overall, it can be observed from these tables that KNN regression outperformed here over all the datasets.

For better visibility, we summarize Tables S4, S5 and S6 and compare the results concerning only  $R^2$  in Table 3. The KNN-based regression technique achieved exceptional performance

across all three datasets, achieving  $R^2$  of more than 0.99, in stark contrast to the contemporary regression models, such as ANN, random forest, decision tree, and linear regression. Only in the 2-gases dataset, for chloroform prediction, random forest performed slightly better than KNN regression. The performance of the random forest was also quite similar to the KNN regression here.

Table 3: Comparison of  $R^2$  obtained by employed ML-based regression architectures

Dataset	Gas Name	KNN Regression	ANN	Random Forest	Decision Tree	Linear Regression
1-gas	Acetone	<b>0.99997</b>	0.43819	0.99412	0.71512	0.82034
	Toluene	<b>0.99997</b>	0.00000	0.99348	0.71391	0.81937
	Ethanol	<b>0.99997</b>	0.00000	0.99426	0.71547	0.81945
	Chlorofor m	<b>0.99990</b>	0.99435	0.99428	0.71526	0.82019
2-gases	Acetone	<b>0.99996</b>	0.24191	0.99992	0.88192	0.97698
	Toluene	<b>0.99998</b>	0.39794	0.99993	0.88135	0.97672
	Ethanol	<b>0.99998</b>	0.21728	0.99997	0.87986	0.97710
	Chlorofor m	0.99992	0.99656	<b>0.99993</b>	0.88072	0.97695
3-gases	Acetone	<b>0.99994</b>	0.85374	0.99972	0.92822	0.97455
	Toluene	<b>0.99991</b>	0.48192	0.99984	0.92787	0.97506

	Ethanol	<b>0.99992</b>	0.66963	0.99989	0.92846	0.97480
	Chlorofor m	<b>0.99976</b>	0.98816	0.99972	0.92783	0.97501

#### 4. Discussion

Although metal oxide thin films are the most successful sensor materials, the major limitation of these materials is their lack of selectivity. The systematic way of characterizing gas sensors devices involves one-by-one exposure to each gas and characterizing the sensitivity as shown in Fig. 1. In such cases, the sensor may show a significantly preferred sensitivity, called selectivity towards a particular gas (like ZnO and NiO shows for ethanol in 1-gas case). However, it gets challenging when another potential interfering gas exists in the atmosphere. Although the other interfering gas may not have high sensitivity in the absence of other gases, it adversely affects the response in otherwise preferred (selective) detection, as seen in Fig. 3. Ethanol gas response when studied in the presence of other single or double gases, the response is substantially reduced (by order of magnitude). Therefore, using conventional analysis methods, gas mixtures are challenging to analyze using a single sensor or even with an array of sensors. Albeit, the sensors utilized in the study are robust and sensitive and show good microstructural traits as required for an ideal metal oxide material for high responsivity[46, 58].

We employed ML-based methods to analyze the sensor array response of such a complex mixture where there is maximum cross-reactivity for one sensor (CuO) while the other two show some preferred selectivity (NiO and ZnO) towards ethanol. Our analysis involved ML algorithms like RF, KNN, Decision Tree, Linear Regression, Logistic Regression, Naive

Bayes, LDA, ANN, and SVM. Among these, RF and KNN gave the best results with extraordinary accuracy of more than 99%. The algorithms could classify and identify the gas type and reasonably estimate the gas concentration of the varying chemicals for 1-gas, 2-gases and 3-gases datasets.

The level of complexity of data and the resources used, such as no of sensors in the array, no of gases studied, the model used and the complexity of data in this study have been compared with that of other studies reported in the literature. For instance, Djedidi O. *et al.*[59] created a method to use a single temperature-modulated MOS sensor and a data-driven model to detect and identify various gas species and their mixtures. By taking the characteristics from dynamic curves and introducing a four-sensor array, Chu J. *et al.*[59] could distinguish between 11 different NO<sub>2</sub> and CO mixes and identifies different target gases using BPNN. The categorization of VOC species and concentrations using a 108-device graphene-based sensor array swept at high speeds has been shown in the study conducted by Capman N S S. *et al.*[60]. To increase selectivity, the array was functionalized with 36 different chemical receptors. All devices were virtually probed simultaneously to gather a cross-reactive data set for ML algorithms. To discriminate between 5 distinct reducing gases, two multi-sensor chips made of SnO<sub>2</sub> NWs covered with Ag and Pt NPs were combined by Thai N X. *et al.*[61]. The "brain" of the system (based on the SVM) is trained using a first dataset of 4D points, and the sensor performance is tested using any subsequent point. With practical machine learning algorithms and MDS (Molecular Dynamic Simulations), Huang S. *et al.*[62] have shown an ultrasensitive, highly discriminative graphene nanosensing platform for detecting and identifying NH<sub>3</sub> and PH<sub>3</sub> at room temperature. Kanaparthi. *et al.*[63] have developed an analytical technique that uses a single chemiresistive ZnO gas sensor to detect NH<sub>3</sub>, CO<sub>2</sub> and H<sub>2</sub>S gases selectively at significantly low power consumption. In order to anticipate the gas present in the air, ML techniques including NB, LR, SVM and RF were used for the data comprised of sensor

responses and ternary logic. Over a single chemiresistive sensor, Acharya S. and coworkers[64] used signal transform methods combined with ML technologies, which allowed for accurate quantification and selective identification of the tested VOCs. The feature extraction technique suggested in the study by Xu Y. *et al.*[65] is based on KPCA. Qualitative identification of mixed gas is made possible by the binary mixed gas identification model of the KNN classification method. A regression approach based on MVRVM was suggested to obtain quantitative gas concentration detection for the qualitative identification findings. Sett A. *et al.*[66] used ZnO nanorods to create a susceptible, stable, and reliable VOC sensor. In reaction to three VOCs, the sensor showed high responsiveness and stability. Features were taken out and supplied into PCA as input. Ref[67] shows that applying statistical shape space pre-processing to the signal of temperature-modulated metal oxide gas sensors improves the selectivity of gas identification with an ANN-based ML algorithm compared to other signal processing methods like PCA, DWT, polynomial curve fitting, and data normalization. Intrinsic CuO and ZnO heterostructures with different weight percentages of CuO–ZnO were made and used as resistance sensors to find four volatile organic compounds. The SVM algorithm with stacked k-fold cross-validation was used for classification, and for measurement, the MLR method was used[68]. On the other hand, in this work, we have used only three sensors that operate at the same temperature and show a distinct mix of selective (NiO and ZnO) and non-selective sensors (CuO) for ethanol vapors. Using two algorithms we obtained the best possible classification (qualitative) and regression (quantitative) identification of gases. Moreover, the gases identified in the study are highly likely to indicate underlying physiological conditions in several diseases. Therefore, sensor and analysis studies have high significance for biomedical diagnostics and point-of-care devices. In Table 4, we present a brief comparison with some state-of-the-art methods.

Table 4: Comparative analysis with some state-of-the-art studies.

No. of sensors	No. of gases together	Comple xity	Models Used	Ref.
1 (WO <sub>3</sub> )	3 (CO, O <sub>3</sub> , NO <sub>2</sub> )	Medium	SVM	55
4 (Commercial MOS Sensors TGS 2600, TGS2602, TGS 2610, TGS 2620)	2 (NO <sub>2</sub> , CO)	Medium	BPNN + CNN	56
1 (Graphene)	36 VOC Receptors	High	PCA + RF	57
1 (SnO <sub>2</sub> Nanowires)	5 (Acetone, Ammonia, H <sub>2</sub> , H <sub>2</sub> S, Ethanol)	Medium	SVM	58
1 (Graphene)	2 (NH <sub>3</sub> , PH <sub>3</sub> )	Low	PCA + LDA	59
1 (ZnO)	3 ( <i>separate</i> ) (H <sub>2</sub> S, NH <sub>3</sub> , CO <sub>2</sub> )	Low	NB + LR + SVM + RF	60
1 (SnO <sub>2</sub> )	4( <i>separate</i> ) (Formaldehyde, Methanol, Propanol, Toluene)	Low	FFT + DWT (SVM + RF + MLP)	61

<b>5</b> (Commercial MOS Sensors TGS2600, TGS2610, TGS2611, TGS2602, TGS2620)	<b>2</b> (CH <sub>4</sub> , CO)	Medium	PCA + ICA + KPCA + KNN + MVRVM	62
<b>1</b> (ZnO)	<b>7</b> (separate) (Toluene, Acetone, NH <sub>3</sub> , Ethanol, 2-Propanol, Formaldehyde, Methanol)	Low	PCA	63
<b>3</b> (SnO <sub>2</sub> , Au/ SnO <sub>2</sub> , AuPd/ SnO <sub>2</sub> )	<b>2</b> ( Methane, Propane)	Medium	SSA	64
<b>3</b> (CuO, ZnO, CuO-ZnO)	<b>4</b> (Methanol, Acetonitrile, Isopropanol, Toluene)	Low	t-SNE + SVM	65
<b>3</b> (ZnO, NiO, CuO)	<b>4</b> (Ethanol, Acetone, Toluene, Chloroform)	Medium	KNN + ANN + RF +DT + LiR + LR +NB + LDA	This work
<b>SVM:</b> Support Vector Machine, <b>BPNN:</b> Back Propagation Neural Network, <b>CNN:</b> Convolutional Neural Network, <b>PCA:</b> Principal Component Analysis, <b>RF:</b> Random Forest, <b>LDA:</b> Linear Discriminant Analysis, <b>NB:</b> Naïve Bayes, <b>LR:</b> Logistic Regression, <b>FFT:</b>				

*Fast Fourier Transform , **DWT**: Discrete Wavelet Transform , **MLP**: Multi Layer Perceptron, **ICA**: Independent Component Analysis, **KPCA**: Kernel Principal Component Analysis, **KNN**: K-Nearest Neighbors, **MVRVM**: Multivariate Relevance Vector Machine, **SSA**: Statistical Shape Analysis, **t-SNE**: t-Distributed Stochastic Neighbor Embedding, **DT**: Decision Tree, **LiR**: Linear Regression, **ANN**: Artificial Neural Network.*

## 5. Conclusion

In this study, we fabricated a gas sensor array consisting of three metal oxides, i.e., ZnO, NiO and CuO. Each sensor in the array was extensively characterized using state-of-the-art surface and material characterization techniques (e.g., SEM and XRD). Each of these materials is highly responsive to a large number of gases, generating cross-reactive and complex chemiresistive signals, which is a boon as well as a bane at the same time as it can be used to detect many gases; nevertheless, they would lack conclusiveness. To handle such complex data set, ML algorithms have been used to classify and predict the levels of individual gases in mixtures. To get the best algorithms out of several that we tried, the parameters of the algorithms have been extensively optimized toward the classification and prediction of different analyte gases. We anticipate that the proposed sensor array can be used for the analysis of different VOCs in complex mixtures (e.g., breath) for non-invasive diagnostic of disease and its monitoring at the point-of-care. In our future studies, we plan to miniaturize the proposed sensor array and modify the sensor surface with different nanomaterial-based coatings to enhance the signal-to-noise ratio and to generate a variable data set from complex mixtures that will further be analyzed using advanced ML algorithms to classify and predict the individual gas levels in complex mixtures. The developed sensor array will be used to diagnose different diseases at the point-of-need non-invasively, which can improve the quality

of life of individuals by reducing the cost of diagnostics and treatment monitoring of certain disease, and time of diagnostics by enabling on-site disease diagnostics capabilities.

## **Supplementary Material**

The Supplementary Material includes the sample fabrication details, the device design, the I-V characteristics, The Gas sensing data as well as the different ML model parameters, etc.

## **Acknowledgment**

The authors are thankful to SERB core research grant (CRG/2022/006973) Govt. of India for the funding support received. The Central Instrumentation Facility of IISER Thiruvananthapuram is also acknowledged for the XRD and SEM facilities.

## **Data availability statement**

The data is available with the corresponding author upon reasonable request.

## **Conflict of Interest**

The authors declare no conflict of interest.

## **References**

- [1] Wang P, Huang Q, Meng S, Mu T, Liu Z, He M, Li Q, Zhao S, Wang S and Qiu M 2022 Identification of lung cancer breath biomarkers based on perioperative breathomics testing: A prospective observational study *EClinicalMedicine* **47**
- [2] Bos L D J, Weda H, Wang Y, Knobel H H, Nijzen T M E, Vink T J, Zwinderman A H, Sterk P J and Schultz M J 2014 Exhaled breath metabolomics as a noninvasive diagnostic tool for acute respiratory distress syndrome *European Respiratory Journal* **44** 188-97

- [3] Das S and Pal M 2020 Non-invasive monitoring of human health by exhaled breath analysis: A comprehensive review *Journal of The Electrochemical Society* **167** 037562
- [4] Issitt T, Wiggins L, Veysey M, Sweeney S T, Brackenbury W J and Redecker K 2022 Volatile compounds in human breath: critical review and meta-analysis *Journal of Breath Research* **16** 024001
- [5] Haick H, Broza Y Y, Mochalski P, Ruzsanyi V and Amann A 2014 Assessment, origin, and implementation of breath volatile cancer markers *Chemical Society Reviews* **43** 1423-49
- [6] Ates H C and Dincer C 2023 Wearable breath analysis *Nature Reviews Bioengineering* **1** 80-2
- [7] Sempionatto J R, Lasalde-Ramírez J A, Mahato K, Wang J and Gao W 2022 Wearable chemical sensors for biomarker discovery in the omics era *Nature Reviews Chemistry* **6** 899-915
- [8] Long Y, Wang C, Wang T, Li W, Dai W, Xie S, Tian Y, Liu M, Liu Y and Peng X 2020 High performance exhaled breath biomarkers for diagnosis of lung cancer and potential biomarkers for classification of lung cancer *Journal of Breath Research* **15** 016017
- [9] Hermawan A, Amrillah T, Riapanitra A, Ong W-J and Yin S 2021 Prospects and Challenges of MXenes as Emerging Sensing Materials for Flexible and Wearable Breath-Based Biomarker Diagnosis *Advanced Healthcare Materials* **10** 2100970
- [10] Freddi S, Emelianov A V, Bobrinetskiy I I, Drera G, Pagliara S, Kopylova D S, Chiesa M, Santini G, Mores N, Moscato U, Nasibulin A G, Montuschi P and Sangaletti L 2020 Development of a Sensing Array for Human Breath Analysis Based on SWCNT Layers Functionalized with Semiconductor Organic Molecules *Advanced Healthcare Materials* **9** 2000377

[11] Shirasu M and Touhara K 2011 The scent of disease: volatile organic compounds of the human body related to disease and disorder *The Journal of Biochemistry* **150** 257-66

[12] Bhandari M P, Polaka I, Vangrav R, Mezmale L, Veliks V, Kirshners A, Mochalski P, Dias-Neto E and Leja M 2023 Volatile Markers for Cancer in Exhaled Breath—Could They Be the Signature of the Gut Microbiota? *Molecules* **28** 3488

[13] Rymarczyk T, Stanikowski A and Nita P 2019 Wearable sensor array for biopotential measurements (9-12 June 2019) p 184-7

[14] Dixit K, Fardindoost S, Ravishankara A, Tasnim N and Hoorfar M 2021 Exhaled Breath Analysis for Diabetes Diagnosis and Monitoring: Relevance, Challenges and Possibilities *Biosensors* **11** 476

[15] Spacek L A, Mudalel M L, Lewicki R, Tittel F K, Risby T H, Stoltzfus J, Munier J J and Solga S F 2015 Breath ammonia and ethanol increase in response to a high protein challenge *Biomarkers* **20** 149-56

[16] Solga S F, Alkhuraishe A, Cope K, Tabesh A, Clark J M, Torbenson M, Schwartz P, Magnuson T, Diehl A M and Risby T H 2006 Breath biomarkers and non-alcoholic fatty liver disease: Preliminary observations *Biomarkers* **11** 174-83

[17] Wang C, Mbi A and Shepherd M 2010 A Study on Breath Acetone in Diabetic Patients Using a Cavity Ringdown Breath Analyzer: Exploring Correlations of Breath Acetone With Blood Glucose and Glycohemoglobin A1C *IEEE Sensors Journal* **10** 54-63

[18] Turner C, Walton C, Hoashi S and Evans M 2009 Breath acetone concentration decreases with blood glucose concentration in type I diabetes mellitus patients during hypoglycaemic clamps *Journal of Breath Research* **3** 046004

[19] Lin X, Xu Y, Pan X, Xu J, Ding Y, Sun X, Song X, Ren Y and Shan P-F 2020 Global, regional, and national burden and trend of diabetes in 195 countries and territories: an analysis from 1990 to 2025 *Scientific Reports* **10** 14790

[20] Jo W K, Weisel C P and Lioy P J 1990 Chloroform Exposure and the Health Risk Associated with Multiple Uses of Chlorinated Tap Water *Risk Analysis* **10** 581-5

[21] Fang C, Behr M, Xie F, Lu S, Doret M, Luo H, Yang W, Aldous K, Ding X and Gu J 2008 Mechanism of chloroform-induced renal toxicity: Non-involvement of hepatic cytochrome P450-dependent metabolism *Toxicology and Applied Pharmacology* **227** 48-55

[22] Moon H G, Jung Y, Han S D, Shim Y-S, Shin B, Lee T, Kim J-S, Lee S, Jun S C, Park H-H, Kim C and Kang C-Y 2016 Chemiresistive Electronic Nose toward Detection of Biomarkers in Exhaled Breath *ACS Applied Materials & Interfaces* **8** 20969-76

[23] Liu L, Wang Y, Liu Y, Wang S, Li T, Feng S, Qin S and Zhang T 2022 Heteronanostructural metal oxide-based gas microsensors *Microsystems & Nanoengineering* **8** 85

[24] Guntner A T, Koren V, Chikkadi K, Righettoni M and Pratsinis S E 2016 E-Nose Sensing of Low-ppb Formaldehyde in Gas Mixtures at High Relative Humidity for Breath Screening of Lung Cancer? *ACS Sensors* **1** 528-35

[25] Choi S-J, Ku K H, Kim B J and Kim I-D 2016 Novel Templating Route Using Pt Infiltrated Block Copolymer Microparticles for Catalytic Pt Functionalized Macroporous WO<sub>3</sub> Nanofibers and Its Application in Breath Pattern Recognition *ACS Sensors* **1** 1124-31

[26] Fowler S J and Sterk P J 2019 Breath biomarkers in asthma: we're getting answers, but what are the important questions? : Eur Respiratory Soc)

[27] Wijaya D R, Afianti F, Arifianto A, Rahmawati D and Kodogiannis V S 2022 Ensemble machine learning approach for electronic nose signal processing *Sensing and Bio-Sensing Research* **36** 100495

[28] Haripriya P, Rangarajan M and Pandya H J 2023 Breath VOC analysis and machine learning approaches for disease screening: a review *Journal of Breath Research*

[29] Koutsandreas D, Spiliotis E, Petropoulos F and Assimakopoulos V 2022 On the selection of forecasting accuracy measures *Journal of the Operational Research Society* **73** 937-54

[30] Uhrovčík J 2014 Strategy for determination of LOD and LOQ values – Some basic aspects *Talanta* **119** 178-80

[31] Cho H, Kim Y-j, Jung H J, Lee S-W and Lee J W 2008 OutlierD: an R package for outlier detection using quantile regression on mass spectrometry data *Bioinformatics* **24** 882-4

[32] Dasu T and Johnson T 2003 *Exploratory data mining and data cleaning*: John Wiley & Sons)

[33] Powers D and Xie Y 2008 *Statistical methods for categorical data analysis*: Emerald Group Publishing)

[34] Romero C and Ventura S 2013 Data mining in education *Wiley Interdisciplinary Reviews: Data mining and knowledge discovery* **3** 12-27

[35] Srinatha N, No Y, Kamble V B, Chakravarty S, Suriyamurthy N, Angadi B, Umarji A and Choi W 2016 Effect of RF power on the structural, optical and gas sensing properties of RF-sputtered Al doped ZnO thin films *RSC Advances* **6** 9779-88

[36] Chou M H, Liu S B, Huang C Y, Wu S Y and Cheng C L 2008 Confocal Raman spectroscopic mapping studies on a single CuO nanowire *Applied Surface Science* **254** 7539-43

[37] Chrzanowski J and Irwin J C 1989 Raman scattering from cupric oxide *Solid State Communications* **70** 11-4

[38] Dietz R E, Brinkman W F, Meixner A E and Guggenheim H J 1972 RAMAN SCATTERING BY FOUR MAGNONS IN NiO AND KNiF<sub>3</sub> *AIP Conference Proceedings* **5** 338-

[39] Rammal M B and Omanovic S 2020 Synthesis and characterization of NiO, MoO<sub>3</sub>, and NiMoO<sub>4</sub> nanostructures through a green, facile method and their potential use as electrocatalysts for water splitting *Materials Chemistry and Physics* **255** 123570

[40] Urs Mb K and Kamble V B 2021 Protonic conduction induced selective room temperature hydrogen response in ZnO/NiO heterojunction surfaces *Sensors and Actuators B: Chemical* **348** 130605

[41] Ristić M, Musić S, Ivanda M and Popović S 2005 Sol-gel synthesis and characterization of nanocrystalline ZnO powders *Journal of Alloys and Compounds* **397** L1-L4

[42] Ridhuan N S, Abdul Razak K, Lockman Z and Abdul Aziz A 2012 Structural and morphology of ZnO nanorods synthesized using ZnO seeded growth hydrothermal method and its properties as UV sensing *PloS one* **7** e50405

[43] Selim F A, Weber M H, Solodovnikov D and Lynn K G 2007 Nature of Native Defects in ZnO *Physical Review Letters* **99** 085502

[44] Bandopadhyay K and Mitra J 2015 Zn interstitials and O vacancies responsible for n-type ZnO: what do the emission spectra reveal? *RSC Advances* **5** 23540-7

[45] Deng Y 2019 *Semiconducting Metal Oxides for Gas Sensing*, ed Y Deng (Singapore: Springer Singapore) pp 23-51

[46] Hunter G W, Akbar S, Bhansali S, Daniele M, Erb P D, Johnson K, Liu C-C, Miller D, Oralkan O, Hesketh P J, Manickam P and Vander Wal R L 2020 Editors' Choice—

Critical Review—A Critical Review of Solid State Gas Sensors *Journal of The Electrochemical Society* **167** 037570

- [47] Kleinbaum D G, Klein M and Pryor E R 2002 *Logistic regression: a self-learning text* vol 94: Springer)
- [48] Larose D T and Larose C D 2014 *Discovering knowledge in data: an introduction to data mining* vol 4: John Wiley & Sons)
- [49] Abdi H and Williams L J 2010 Principal component analysis *Wiley interdisciplinary reviews: computational statistics* **2** 433-59
- [50] Rish I 2001 An empirical study of the naive Bayes classifier(vol 3) p 41-6
- [51] Fratello M and Tagliaferri R 2019 *Encyclopedia of Bioinformatics and Computational Biology*, ed S Ranganathan, *et al.* (Oxford: Academic Press) pp 374-83
- [52] Xanthopoulos P, Pardalos P M, Trafalis T B, Xanthopoulos P, Pardalos P M and Trafalis T B 2013 Linear discriminant analysis *Robust data mining* 27-33
- [53] Haykin S 1998 *Neural Networks: A Comprehensive Foundation*: Prentice Hall PTR)
- [54] Kohli S, Godwin G T and Urolagin S 2021 Sales prediction using linear and KNN regression: Springer) p 321-9
- [55] Montgomery D C, Peck E A and Vining G G 2021 *Introduction to linear regression analysis*: John Wiley & Sons)
- [56] Lewis R J 2000 An introduction to classification and regression tree (CART) analysis(vol 14): Citeseer)
- [57] Schmidt-Hieber J 2020 Nonparametric regression using deep neural networks with ReLU activation function
- [58] Korotcenkov G 2007 Metal oxides for solid-state gas sensors: What determines our choice? *Mater. Sci. Eng., B* **139** 1-23

[59] Djedidi O, Djeziri M A, Morati N, Seguin J-L, Bendahan M and Contaret T 2021 Accurate detection and discrimination of pollutant gases using a temperature modulated MOX sensor combined with feature extraction and support vector classification *Sensors and Actuators B: Chemical* **339** 129817

[60] Capman N S S, Zhen X V, Nelson J T, Chaganti V R S K, Finc R C, Lyden M J, Williams T L, Freking M, Sherwood G J, Bühlmann P, Hogan C J and Koester S J 2022 Machine Learning-Based Rapid Detection of Volatile Organic Compounds in a Graphene Electronic Nose *ACS Nano* **16** 19567-83

[61] Thai N X, Tonezzer M, Masera L, Nguyen H, Duy N V and Hoa N D 2020 Multi gas sensors using one nanomaterial, temperature gradient, and machine learning algorithms for discrimination of gases and their concentration *Analytica Chimica Acta* **1124** 85-93

[62] Huang S, Croy A, Panes-Ruiz L A, Khavrus V, Bezugly V, Ibarlucea B and Cuniberti G 2022 Machine Learning-Enabled Smart Gas Sensing Platform for Identification of Industrial Gases *Advanced Intelligent Systems* **4** 2200016

[63] Kanaparthi S and Singh S G 2021 Discrimination of gases with a single chemiresistive multi-gas sensor using temperature sweeping and machine learning *Sensors and Actuators B: Chemical* **348** 130725

[64] Acharyya S, Nag S and Guha P K 2022 Ultra-selective tin oxide-based chemiresistive gas sensor employing signal transform and machine learning techniques *Analytica Chimica Acta* **1217** 339996

[65] Xu Y, Zhao X, Chen Y and Zhao W 2018 Research on a Mixed Gas Recognition and Concentration Detection Algorithm Based on a Metal Oxide Semiconductor Olfactory System Sensor Array *Sensors* **18** 3264

[66] Sett A, Rana T, Roy R, Saha T and Bhattacharyya T K 2020 Selective detection of multiple VOCs employing zinc oxide nanorods and principle component2-4 *Oct. 2020*) p 1-6

[67] Krivetskiy V V, Andreev M D, Efitorov A O and Gaskov A M 2021 Statistical shape analysis pre-processing of temperature modulated metal oxide gas sensor response for machine learning improved selectivity of gases detection in real atmospheric conditions *Sensors and Actuators B: Chemical* **329** 129187

[68] Kulkarni S and Ghosh R 2023 CuO–ZnO p-n junctions for accurate prediction of multiple volatile organic compounds aided by machine learning algorithms *Analytica Chimica Acta* **1253** 341084